Comparison of hyperelastic models for granular materials

Paul W. Humrickhouse,[1,2,*] J. Phil Sharpe,[1] and Michael L. Corradini[2]
[1]*Fusion Safety Program, Idaho National Laboratory, P.O. Box 1625, Idaho Falls, Idaho 83415, USA*
[2]*Department of Engineering Physics, University of Wisconsin, 1500 Engineering Drive, Madison, Wisconsin 53706, USA*
(Received 4 November 2009; published 15 January 2010)

Three recently proposed hyperelastic models for granular materials are compared with experiment data. Though all three are formulated to give elastic moduli that are power law functions of the mean stress, they have rather different dependencies on individual stresses, and generally differ from well established experimental forms. Predicted static stress distributions are in qualitative agreement with experiments, but do not differ greatly from isotropic linear elasticity, and similarly fail to account for variability in experiment data that presumably occurs due to a preparation dependence of granular materials.

DOI: 10.1103/PhysRevE.81.011303 PACS number(s): 45.70.Cc, 46.05.+b, 81.40.Jj, 81.05.Rm

I. INTRODUCTION

Despite their ubiquity in nature and industry, granular materials and their behavior are not always well understood. A striking example is the static stress distribution, easily obtained for conventional materials, but still a topic of some debate for granular materials [1]. Though in most situations plastic deformations dominate in granular materials, the static regime is generally assumed to be elastic, and isotropic linear elasticity (ILE) is sometimes employed. However, stress-strain relations for granular media (even in the small-strain, reversible regime) are known to be nonlinear. Choosing an appropriate form can meet with theoretical difficulties. Zytynski *et al.* [2] noted that such models do not necessarily conserve elastic energy; an incremental stress-strain relation may not even result in a closed cycle of strain when subjected to a closed cycle of stress, giving rise to a sort of "irreversible elasticity." In order to avoid such difficulties, it is necessary to begin with a *hyperelastic* model, in which the elastic constitutive behavior is derived from an appropriate scalar free energy. This approach was advanced by Houlsby and colleagues [3–5], and was incorporated into a thermodynamically consistent elastoplastic framework termed "hyperplasticity" [6].

In the present work, we are interested in the purely elastic regime of dry, cohesionless granular materials, and suitable hyperelastic models that would govern static stress distributions and sound propagation in them. Such materials are known to have elastic moduli that vary with the mean stress, typically $K, G \sim P^{1/2}$, though the Hertz theory for individual particle contacts suggests $K, G \sim P^{1/3}$ [7]. Linear elasticity possesses constant elastic moduli, as it has a quadratic free energy; neglecting temperature (here and throughout), it possesses the Helmholtz free energy $\mathcal{F}$,

$$\mathcal{F} = \frac{1}{2}K\Delta^2 + Gu_s^2 \tag{1}$$

where Δ and u_s^2 are the first and second strain invariants,

$$\Delta \equiv -u_{ii}, \tag{2}$$

$$u_s^2 \equiv u_{ij}^0 u_{ij}^0, \tag{3}$$

$$u_{ij}^0 \equiv u_{ij} - \frac{1}{3}u_{\ell\ell}\delta_{ij}. \tag{4}$$

Equivalently, ILE is defined by the negative Gibbs free energy $\mathcal{G}$,

$$\mathcal{G} = \frac{P^2}{2K} + \frac{\sigma_s^2}{4G} \tag{5}$$

in terms of the stress invariants

$$P \equiv -\frac{1}{3}\sigma_{ii}, \tag{6}$$

$$\sigma_s^2 \equiv \sigma_{ij}^0 \sigma_{ij}^0, \tag{7}$$

$$\sigma_{ij}^0 \equiv \sigma_{ij} - \frac{1}{3}\sigma_{\ell\ell}\delta_{ij}, \tag{8}$$

which may be obtained from Eq. (1) via the Legendre transform [6,8]. The linear stress-strain relation is obtained by differentiating

$$\sigma_{ij} = \frac{\partial \mathcal{F}}{\partial u_{ij}} \tag{9}$$

or

$$u_{ij} = \frac{\partial \mathcal{G}}{\partial \sigma_{ij}}. \tag{10}$$

A suitable nonlinear form, then, should be obtained from an appropriately modified elastic potential. Three such potentials have recently been proposed that are suitable for cohesionless granular materials. The purpose of the present work is to present a comprehensive comparison of these models with experiment data for the stress dependence of elastic moduli, and static stress distributions in various configurations.

*paul.humrickhouse@inl.gov

II. HYPERELASTIC FORMS

A. Granular elasticity

The following Helmholtz free energy has been proposed by Jiang and Liu [9]:

$$\mathcal{F} = \mathcal{A}\Delta^a\left(\frac{2}{5}\xi\Delta^2 + u_s^2\right). \tag{11}$$

This is the quadratic form of the free energy of ILE, multiplied by Δ^a; the two elastic constants are $\mathcal{A}$ (units of stress) and ξ (dimensionless). Such a modification will give elastic moduli that are power law functions of the strains, or stresses; Jiang and Liu take $a=1/2$ (consistent with "Hertz contacts," $K, G \sim P^{1/3}$) and call this "granular elasticity," or GE, given by the free energy

$$\mathcal{F} = \mathcal{A}\sqrt{\Delta}\left(\frac{2}{5}\xi\Delta^2 + u_s^2\right). \tag{12}$$

A large body of experiment data, on the other hand, suggest $K, G \sim P^{1/2}$, implying $a=1$. This gives a free energy cubic in the strains,

$$\mathcal{F} = \mathcal{A}\left(\frac{2}{5}\xi\Delta^3 + \Delta u_s^2\right), \tag{13}$$

which we refer to as GE-cubic or GE-C. We investigate both choices in what follows; the discrepancy has been given various micro-mechanical interpretations in the literature [10,11].

Jiang and Liu have examined GE in a series of papers [9,12–17], and found it to exhibit a number of desirable features for granular materials, which we briefly summarize here. Recalling that $\Delta=-u_{ii}$ will be positive in compression, it is immediately apparent that, due to the $\sqrt{\Delta}$ terms, there are no tensile solutions. The nonlinear form also results in a coupling between shear and volumetric stresses and strains

$$P \equiv \frac{\partial \mathcal{F}}{\partial \Delta} = \frac{2}{5}\mathcal{A}\xi(a+2)\Delta^{a+1} + a\mathcal{A}\frac{u_s^2}{\Delta^{1-a}}, \tag{14}$$

$$\sigma_s \equiv \frac{\partial \mathcal{F}}{\partial u_s} = 2\mathcal{A}\Delta^a u_s. \tag{15}$$

Solving the above for $\Delta(u_s, P)$ and plotting u_s vs Δ at different values of P [9,17] reveals shear dilatancy: the compression Δ decreases with increasing shear u_s.

Perhaps the most interesting feature of GE, and unique to it among the models considered here, is the prediction of a mechanically unstable region. Stability requires that the free energy $\mathcal{F}$ be a convex function of the strains [8]:

$$\frac{\partial^2 \mathcal{F}}{\partial \Delta^2} \geq 0, \tag{16}$$

$$\frac{\partial^2 \mathcal{F}}{\partial u_s^2} \geq 0, \tag{17}$$

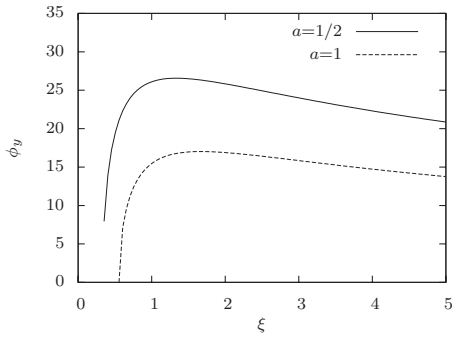

FIG. 1. The yield angle ϕ_y for GE as a function of ξ. The maximum occurs at ~26.5° for $a=1/2$ and ~17° for $a=1$.

$$\frac{\partial^2 \mathcal{F}}{\partial \Delta^2}\frac{\partial^2 \mathcal{F}}{\partial u_s^2} - \left(\frac{\partial^2 \mathcal{F}}{\partial \Delta\, \partial u_s}\right)^2 \geq 0. \tag{18}$$

In linear elasticity, the first two conditions require that the elastic moduli are positive, in which case the third condition is satisfied as well. Similarly for GE, ξ and $\mathcal{A}$ must be positive, but the third condition gives an additional constraint [9,14,16,17],

$$\frac{u_s^2}{\Delta^2} < \frac{2\xi(a+2)}{5a}. \tag{19}$$

Noting that the stress invariants are given by Eqs. (14) and (15), the stability limit can be rewritten in terms of the stresses,

$$\frac{\sigma_s}{P} = \sqrt{\frac{5}{2\xi a(a+2)}}. \tag{20}$$

This is precisely the Drucker-Prager yield criterion [18]. It should be noted that this limit on the ratio of stress invariants is not the same as the ratio of shear to normal stress components on a plane that defines the Coulomb condition and the friction angle,

$$\left|\frac{\tau_n}{\sigma_n}\right| \leq \mu_f = \tan\,\phi. \tag{21}$$

An expression for the yield angle can be obtained, though, by considering an inclined granular layer, infinite in two directions. Solution of this problem [9,19,20] gives a yield angle in terms of only the constant ξ and exponent a,

$$\tan\,\phi_y = \frac{\sqrt{\dfrac{\xi(a+2)}{5a}} - \dfrac{1}{3}}{\dfrac{2}{5}\xi(a+2) + \dfrac{2}{3}}. \tag{22}$$

The unexpected feature of this relation is a peak in ϕ_y when plotted against ξ (Fig. 1). Though it is stated elsewhere [14,16] that $\xi=5/3$ coincides with $\phi_y=28°$, the peak for GE ($a=1/2$) is $\phi_y \approx 26.5°$ at $\xi=4/3$. Furthermore, while one might expect higher yield angles for "real" (e.g., nonspherical or irregular) materials, taking $a=1$ to better match experiment data shifts the curve even lower, peaking at $\xi=5/3$, $\phi_y \approx 17°$. Generalizations of the Jiang-Liu form were inves-

tigated in [20], including an extension with an additional dependence on the third strain invariant, but none of these alleviated this difficulty.

The yield angle curve is open to some interpretation, as the infinite plane assumption implies zero normal strain in the infinite directions. The stress state will be more complicated in a finite system, say an inclined box, and presumably not analytically tractable. Experiments do indicate that the presence of side walls can increase the yield angle [21,22]. But in both cases, yield angles approached an asymptotic value as the system size increased, so we expect that the limit of infinite extent should, in fact, give a reasonable estimate of the yield angle, provided that the system is large relative to the grain size. But it is not clear how GE might be modified to allow for higher angles.

B. Model of Einav and Puzrin

Similar arguments were employed by Einav and Puzrin (EP), who proposed a nonlinear form of the Gibbs free energy [23]. This approach is advantageous in that it gives the elastic moduli as explicit functions of stresses rather than strains, making for a more straightforward comparison with experiments. A special case of their general form for the negative Gibbs free energy ($\mathcal{G}$) appropriate for cohesionless dry granular materials is

$$\mathcal{G} = \sqrt{\frac{1}{PB}}(\beta P^2 + \sigma_s^2). \tag{23}$$

Here we use the same notation as for GE, and employ two constants β (dimensionless) and B (units of stress). This particular form is chosen to give elastic moduli with the familiar $P^{1/2}$ dependence found in experiments. While this is the same sort of modification applied to the Helmholtz free energy in GE, the two are not equivalent; complementary potentials can in principle be obtained via the Legendre transform, though there is no closed form solution for the Gibbs free energy for GE, or the Helmholtz free energy for EP.

Stability requires that the Gibbs free energy be a concave function of the stress, or equivalently that the negative Gibbs free energy $\mathcal{G}$ be convex. So we require

$$\frac{\partial^2 \mathcal{G}}{\partial P^2} \geq 0, \tag{24}$$

$$\frac{\partial^2 \mathcal{G}}{\partial \sigma_s^2} \geq 0, \tag{25}$$

$$\frac{\partial^2 \mathcal{G}}{\partial P^2}\frac{\partial^2 \mathcal{G}}{\partial \sigma_s^2} - \left(\frac{\partial^2 \mathcal{G}}{\partial P\, \partial\, \sigma_s}\right)^2 \geq 0. \tag{26}$$

Positive constants B and β are sufficient to satisfy all three; thus, EP does not possess the mechanically unstable region of GE.

While $\mathcal{G}$ lacks this stability constraint, it does possess a Drucker-Prager type limit. Identifying

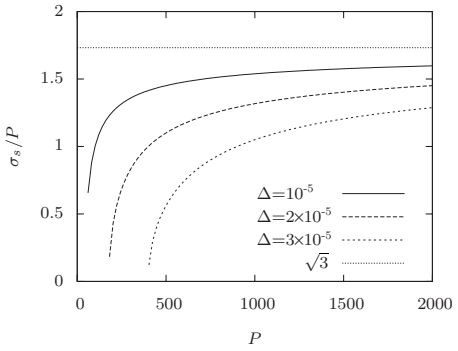

FIG. 2. The stress ratio σ_s/P as a function of pressure, for $\beta=1$ and $B=10^{12}$ (arbitrary units).

$$\frac{\partial \mathcal{G}}{\partial P} = \Delta = \frac{3}{2}\beta\left(\frac{P}{B}\right)^{1/2} - \frac{\sigma_s^2}{2B^{1/2}P^{3/2}} \tag{27}$$

and solving for σ_s,

$$\sigma_s = \sqrt{3\beta P^2 - 2\Delta B^{1/2}P^{3/2}} \tag{28}$$

or in terms of the stress ratio

$$\frac{\sigma_s}{P} = \sqrt{3\beta - \frac{2\Delta B^{1/2}}{P^{1/2}}}. \tag{29}$$

Assuming Δ is positive to ensure compression rather than tension, there is still a Drucker-Prager type limit on the stress ratio (Fig. 2) given by

$$\lim_{P\to\infty} \frac{\sigma_s}{P} = \sqrt{3\beta}. \tag{30}$$

This was noted by Einav and Puzrin, who also recognized that the shear-volumetric coupling resulting from such a potential is appropriate for granular materials. It can be shown that this coupling similarly results in shear dilatancy [19].

C. Model of Houlsby, Amorosi, and Rojas

The limiting stress ratio was considered undesirable by Houlsby, Amorosi, and Rojas (HAR), who proposed another potential [24]. Citing additionally the desire for ease of manipulation, particularly the ability to convert between Helmholtz and Gibbs free energy forms, they propose raising the entire quadratic expression of ILE to an appropriate power. The special case that gives K, $G \sim P^{1/2}$ can be written

$$\mathcal{F} = A(\alpha\Delta^2 + u_s^2)^{3/2}, \tag{31}$$

where again we employ the notation of GE, using a constant with units of stress (A) [1] and another which is dimensionless (α). This potential has no unstable region as in GE, or limiting stress ratio as in EP. It also allows for tension as well as compression, and shear in the absence of compression ($\sigma_s \neq 0$ when $P=0$), neither of which can occur in dry cohesionless materials. The complementary energy can, however, be

[1]There should be no confusion of the constants A in the HAR model, and $\mathcal{A}$ in GE.

obtained via the Legendre transform [6,24]; in this case it is [19]

$$\mathcal{G} = \frac{2}{3\sqrt{3A}}\left(\frac{1}{\alpha}P^2 + \sigma_s^2\right)^{3/4}. \tag{32}$$

The HAR model also possesses shear-volumetric coupling, leading to shear dilation as with GE and EP [19].

III. ELASTIC MODULI

A. Pressure dependence

It was noted previously that dry, cohesionless granular materials invariably possess elastic moduli that vary approximately as $P^{1/2}$. This sort of stress dependence is built into the GE-C, EP, and HAR models described above. Consider the case of pure compression, in which $\sigma_s, u_s = 0$. The bulk modulus is given by

$$K = \frac{P}{\Delta} = \frac{1}{\Delta}\frac{\partial \mathcal{F}}{\partial \Delta} \tag{33}$$

or equivalently

$$\frac{1}{K} = \frac{\Delta}{P} = \frac{1}{P}\frac{\partial \mathcal{G}}{\partial P}. \tag{34}$$

For the GE-C [Eq. (13)], EP [Eq. (23)], and HAR [Eqs. (31) and (32)] models, this leads to

$$K = \sqrt{\frac{6\xi\mathcal{A}}{5}}\sqrt{P}, \tag{35}$$

$$K = \frac{2\sqrt{B}}{3\beta}\sqrt{P}, \tag{36}$$

$$K = \sqrt{3A}\alpha^{3/4}\sqrt{P}. \tag{37}$$

So all three models give a bulk modulus that indeed varies with the square root of pressure. However, experiments have identified more specific stress dependence, which we investigate in this section. In particular, we may obtain analytical forms from the hyperelastic models and compare directly with the orthotropic compliance matrix,

$$\begin{bmatrix} \frac{1}{E_1} & -\frac{\nu_{21}}{E_2} & -\frac{\nu_{31}}{E_3} & 0 & 0 & 0 \\ -\frac{\nu_{12}}{E_1} & \frac{1}{E_2} & -\frac{\nu_{32}}{E_3} & 0 & 0 & 0 \\ -\frac{\nu_{13}}{E_1} & -\frac{\nu_{23}}{E_2} & \frac{1}{E_3} & 0 & 0 & 0 \\ 0 & 0 & 0 & \frac{1}{G_{12}} & 0 & 0 \\ 0 & 0 & 0 & 0 & \frac{1}{G_{23}} & 0 \\ 0 & 0 & 0 & 0 & 0 & \frac{1}{G_{13}} \end{bmatrix}. \tag{38}$$

As the hyperelastic models have only two elastic constants, they are not inherently *anisotropic*; but as we will see, stress dependence *induces* anisotropy. Thus we can account for stress-induced, but not "fabric," anisotropy with these models.

A well-studied simplification of the above is the triaxial test, in which all three shear stress components are zero. If two horizontal components of normal stress (σ_1 and σ_3) are equal, we may further simplify the compliance matrix to

$$\begin{bmatrix} \frac{1}{E_h} & -\frac{\nu_{vh}}{E_v} & -\frac{\nu_{hh}}{E_h} \\ -\frac{\nu_{hv}}{E_h} & \frac{1}{E_v} & -\frac{\nu_{hv}}{E_h} \\ -\frac{\nu_{hh}}{E_h} & -\frac{\nu_{vh}}{E_v} & \frac{1}{E_h} \end{bmatrix}. \tag{39}$$

Many experiments have been carried out on granular materials in this configuration, all of which find similar stress dependence of the elastic moduli; we compare these to the predictions of the hyperelastic models in what follows.

B. Comparison of theories and experiment

1. Poisson's ratio

It is useful to first consider Poisson's ratio, as it can be related to the dimensionless constants in each of the hyperelastic models. It is apparent from the form of the compliance matrix [Eq. (38)] that

$$\nu_{ij} = -\frac{\frac{\partial^2 \mathcal{G}}{\partial \sigma_j \partial \sigma_i}}{\frac{\partial^2 \mathcal{G}}{\partial \sigma_i^2}}. \tag{40}$$

Thus, we may obtain analytical expressions from the EP and HAR models. For the GE-C model, we have instead the stiffness matrix as a function of the strains, which must be inverted. In every case, the scale constants ($\mathcal{A}$, A, and B) cancel, so Poisson's ratio depends only on the stresses and the dimensionless constants ξ, α, and β. In the limit of isotropic stress, all stress dependence cancels, and so, for the EP and HAR models, the experimental data on Poisson's ratio should give some idea what an appropriate range of values is for β and α. For GE-C, $\xi = 5/3$ is fixed in order to maximize the yield angle.

For the case of isotropic stress, $\sigma_1 = \sigma_2 = \sigma_3$, all three models give a constant Poisson's ratio,

$$\nu_{iso} = \frac{18\xi - 5}{36\xi + 5}, \tag{41}$$

$$\nu_{iso} = \frac{8 - \beta}{16 + \beta}, \tag{42}$$

$$\nu_{iso} = \frac{6\alpha - 1}{12\alpha + 1}, \tag{43}$$

for the GE-C, EP, and HAR models, respectively. Some experimental data indicate ν_{iso} is as small as 0.1–0.2, for ex-

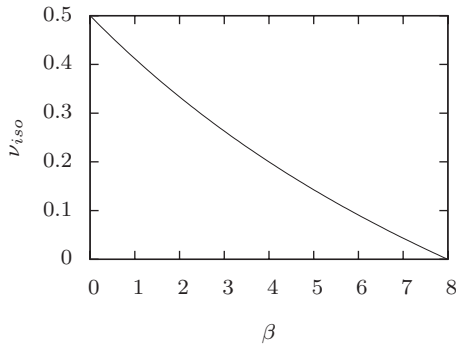

FIG. 3. The isotropic Poisson's ratio as a function of dimensionless material constant β in the EP model.

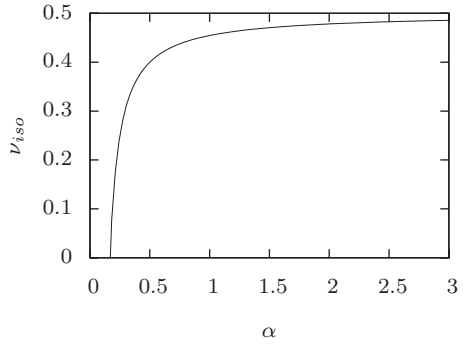

FIG. 4. The isotropic Poisson's ratio as a function of dimensionless material constant α in the HAR model.

ample $\nu_{iso}=0.163$ [25]. For GE-C, this implies $\xi\approx 0.479$, for which there are no solutions (Fig. 1); thus we see that the stress limits imposed by this model can be restrictive. For the EP and HAR models, there are no such restrictions, and we are free to choose β and α to match experimental values of Poisson's ratio. The isotropic values given above provide some idea what range of values for α and β are appropriate for real materials. We do not in practice encounter negative Poisson's ratios in granular materials, so we do not expect $\beta>8$ or $\alpha<1/6$. For isotropic, linear elastic materials, stability requires $\nu\leq 0.5$; there is no such restriction on anisotropic materials, and some values of ν greater than 0.5 have been observed [26]. The isotropic value is typically lower, however, than 0.5. For the EP model this merely implies $\beta>0$, which is already required for stability. The relationship between β and ν_{iso} is plotted in Fig. 3. ν_{iso} is equal to 0.5 in the limit $\alpha\to\infty$ in the HAR model, though it reaches a value of 0.44 at $\alpha=2$ (Fig. 4). So, $1/6<\alpha<2$ may be taken as an approximate range of validity.

2. Young's modulus

Experiments find that the Young's moduli are not just functions of the mean stress, but of the stress in a particular direction. More precisely, Young's modulus in a given direction is a power law function of the normal stress in that direction, but is *independent* of all other stresses. The experimental data are well fitted by the following expressions:

$$E_v = C_v \sigma_v^n, \tag{44}$$

$$E_h = C_h \sigma_h^n, \tag{45}$$

where n is never far from 1/2 [25–36], and here the constants C must have units of $P^{1/2}$. $C_v\neq C_h$ implies some degree of fabric anisotropy, as then $E_v\neq E_h$ even when $\sigma_v=\sigma_h$; conversely, if $C_v=C_h$, the Young's moduli are equal if the stresses are equal, but anisotropic stress states induce anisotropy.

From Eq. (38), it is apparent that for Gibbs free energy models, Young's modulus is given analytically by

$$E_i = \frac{1}{\dfrac{\partial^2 \mathcal{G}}{\partial \sigma_i^2}}.$$

The resulting expressions for the EP and HAR models, respectively, are

$$\frac{E_v}{B} = \frac{4\sqrt{3}\left(2\dfrac{\sigma_h}{B}+\dfrac{\sigma_v}{B}\right)^{5/2}}{(\beta+6)\left(\dfrac{\sigma_v}{B}\right)^2+(4\beta+36)\left(\dfrac{\sigma_v}{B}\right)\left(\dfrac{\sigma_h}{B}\right)+(4\beta+102)\left(\dfrac{\sigma_h}{B}\right)^2} \tag{46}$$

$$\frac{E_v}{A} = \frac{18\alpha^{3/4}\left((6\alpha+1)\left(\dfrac{\sigma_v}{A}\right)^2+(-12\alpha+4)\left(\dfrac{\sigma_v}{A}\right)\left(\dfrac{\sigma_h}{A}\right)+(6\alpha+4)\left(\dfrac{\sigma_h}{A}\right)^2\right)^{5/4}}{(36\alpha^2+12\alpha+1)\left(\dfrac{\sigma_v}{A}\right)^2+(-72\alpha^2+12\alpha+4)\left(\dfrac{\sigma_v}{A}\right)\left(\dfrac{\sigma_h}{A}\right)+(36\alpha^2+84\alpha+4)\left(\dfrac{\sigma_h}{A}\right)^2} \tag{47}$$

For GE and related Helmholtz free energy models, the situation is more complicated. Here we have a stiffness matrix of strain dependent terms, and equations for the stresses σ_v and σ_h, also in terms of the strains. There are not simple expressions for Young's moduli as functions of stress, but inverting the stiffness matrix gives E_v and E_h in terms of the strains. With σ_v, σ_h, E_v, and E_h given as functions of the strains, we may plot their relationship parametrically.

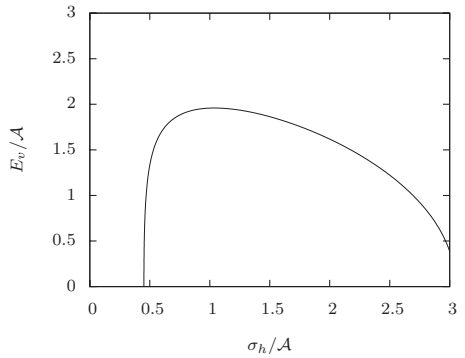

FIG. 5. The vertical Young's modulus E_v as a function of the horizontal stress σ_h for the GE-C model; $\sigma_v/A=1$ and $\xi=5/3$. E_v varies substantially with σ_h, in contrast with experiment data.

A noteworthy aspect of the experiment data fits [Eqs. (44) and (45)] is the assumption that the vertical Young's modulus is a function of *only* the vertical stress, and similarly the horizontal Young's modulus is a function of *only* the horizontal stress. This independence is not present in the hyperelastic models, for which each Young's modulus depends on all the stress components. It should at least be preferred that the Young's modulus in a given direction depends only weakly on the stresses perpendicular to that direction. Consider, then, the expressions for E_v resulting from the hyperelastic models. The parametric plot for GE-C is shown in Fig. 5, and Eqs. (46) and (47) for the EP and HAR models are shown in Figs. 6 and 7. It is apparent that both the GE-C and HAR models predict significant variations in E_v with σ_h, in contrast with experiment data. The GE-C model gives a particularly sharp drop at the limits of stability; it should be noted that stress ratios outside the range plotted in Fig. 5 mark, approximately, the observed limits of the elastic regime [36]. In the EP model, though E_v is not explicitly independent of σ_h, there is very little variation over the entire range of stress ratios in the elastic regime.

Of course, in addition to this independence, we expect that Young's modulus should vary approximately with the square root of the in-plane normal stress component, as observed in experiments [Eqs. (44) and (45)]. The EP and HAR expressions for E_v are plotted against σ_v in Figs. 8 and 9, and

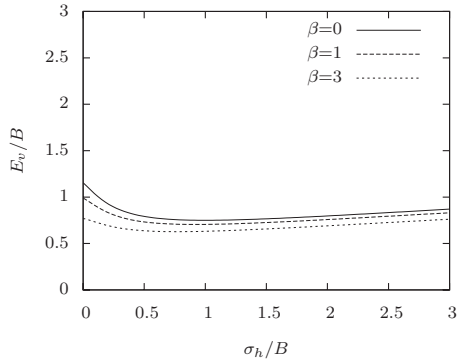

FIG. 6. The vertical Young's modulus E_v as a function of the horizontal stress σ_h for the EP model, $\sigma_v/B=1$. E_v varies only slightly with σ_h, in relative agreement with experiment data, where there is no dependence of E_v on σ_h.

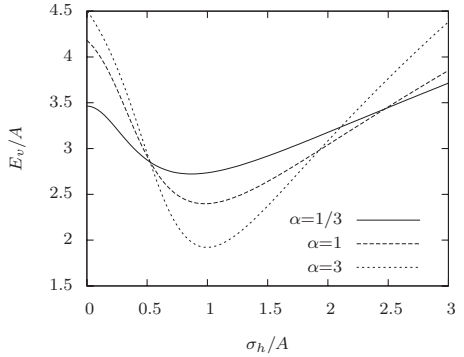

FIG. 7. The vertical Young's modulus E_v as a function of the horizontal stress σ_h for the HAR model, $\sigma_v/A=1$. E_v varies substantially with σ_h, in contrast with experiment data. In particular, the variation increases for increasing values of α.

the parametric plot for GE-C is shown in Fig. 10. The scaling here is arbitrary, so it is the shape, not the magnitude, of the curves that is of interest. While none of the models are exactly linear on the log-log plots, it is clear that the EP model is the best of the three at capturing this behavior. The HAR model is a worse match to experiment data for increasing values of α, and once again we have fixed $\xi=5/3$ for GE-C in order to achieve the maximum yield angle of $\sim 17°$.

3. Shear modulus

Finally, we consider the shear modulus obtained from the models and experiments. This is frequently measured by shear wave propagation in a triaxial or other specimen. The shear modulus is identified as

$$G_{ij} = \frac{1}{\dfrac{\partial^2 \mathcal{G}}{\partial \tau_{ij}^2}} \tag{48}$$

according to Eq. (38). This results in a shear modulus for the EP model of

$$G = \frac{\sqrt{BP}}{4}. \tag{49}$$

There is no stress-induced anisotropy in the shear moduli in this case, i.e.,

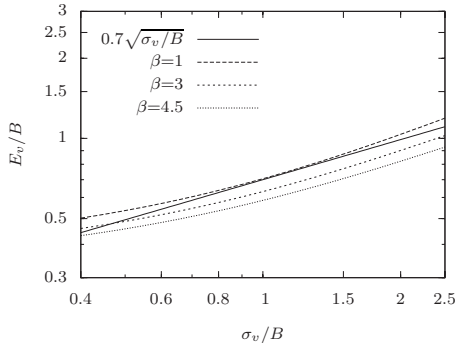

FIG. 8. E_v vs σ_v for the EP model, and experiment fit.

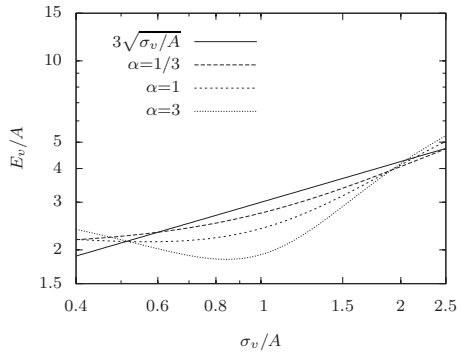

FIG. 9. E_v vs σ_v for the HAR model, and experiment fit.

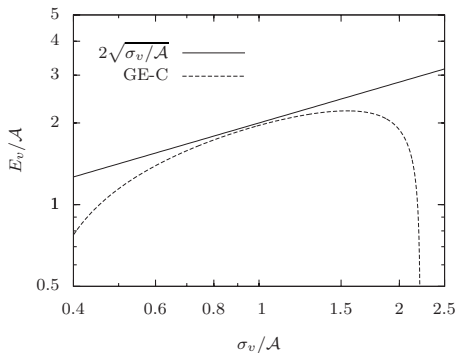

FIG. 10. E_v vs σ_v for the GE-C model, and experiment fit.

$$G = G_{12} = G_{23} = G_{13}. \tag{50}$$

The shear modulus is simply proportional to the square root of the mean normal stress P. This, of course, was the idea behind all the hyperelastic forms presented here, and the shear modulus (just as with the bulk and Young's moduli) does take this form when plotted against the mean stress. Roesler [37] and others [28,29,31,36,38], however, find a more specific relationship between the shear modulus and stress; they find that the shear modulus does not depend on the normal stress acting on the plane of shear, e.g.,

$$G_{12} \neq f(\sigma_{33}) \tag{51}$$

and is a function of only the other two normal stresses, e.g.,

$$G_{12} \sim (\sigma_{11}\sigma_{22})^{1/4}. \tag{52}$$

The HAR model has an additional dependence on the shear stress,

$$G_{ij} = \frac{\sqrt{3A}\left(\frac{1}{\alpha}P^2 + \sigma_s^2\right)^{5/4}}{2\left(\tau_{ij}^2 + \frac{1}{\alpha}P^2 + \sigma_s^2\right)} \tag{53}$$

as does GE [16]. All three models predict the same dependence of the shear modulus on each component of normal stress. It should be noted that shear moduli with different dependence on the normal stress components can only be obtained from a free energy that also depends on the third stress (or strain) invariant.

IV. STRESS DISTRIBUTIONS

GE has been implemented in finite element codes and used to calculate stress distributions in sand piles [14], silos, and granular layers subject to a point load [15], and agrees relatively well with experiment data. As the EP and HAR models are not as extensively tested, they have been implemented (along with GE) in the finite element code Abaqus [39] and are compared against the same sets of experiment data here. Note that in this section we revert to using GE (with $a=1/2$) rather than GE-C (with $a=1$) in order to make a direct comparison with published results for GE [14,15].

A. Abaqus Implementation of nonlinear elastic models

One may implement any desired material behavior in Abaqus through the user material (UMAT) subroutine. In the present case of nonlinear, small strain elasticity, this simply requires providing the stiffness matrix, which may be any function of stresses, strains, or both (and, in principle, any other variable). For GE and HAR, this is straightforward; as both possess a closed form of the Helmholtz free energy, the stiffness matrix may be obtained by differentiating,

$$M_{ijk\ell} = \frac{\partial^2 \mathcal{F}}{\partial u_{ij}\,\partial u_{k\ell}}. \tag{54}$$

For the EP model, differentiating the Gibbs free energy gives the compliance matrix,

$$C_{ijk\ell} = \frac{\partial^2 \mathcal{G}}{\partial \sigma_{ij}\,\partial \sigma_{k\ell}}. \tag{55}$$

The compliance matrix must be inverted to obtain the stiffness matrix for Abaqus, which gives the stiffness matrix in terms of the stresses, whereas the stiffness matrix obtained directly from the Helmholtz free energy in GE and HAR is a function of the strains. Either is equally acceptable for Abaqus. The three problems of interest can all be treated with either plane strain or axisymmetric simplifications, in which there is only one component of shear stress and shear strain.

B. Sand piles and the stress dip

First we turn our attention to the sand pile experiments of Vanel *et al.* [40]. They found a dip in the vertical stress beneath the center of conical and wedge shaped piles poured from a point source, but not for those poured rainlike from a sieve. GE reasonably matches the cases without a stress dip [14], so we shall make the same comparison with the EP and HAR models here. The piles considered by Vanel *et al.* are 8 cm high, 26 cm in diameter or width, and 20 cm thick in the case of the wedge. The density of the material is not reported, and results are normalized with respect to it. Following Krimer *et al.* [14], the density is taken here to be 2660 $\mathrm{kg/m^3}$, typical of the sand used in experiments [36]. At the bottom of the pile, the r and z displacements are set to zero. In addition to gravity, a small pressure is applied to the

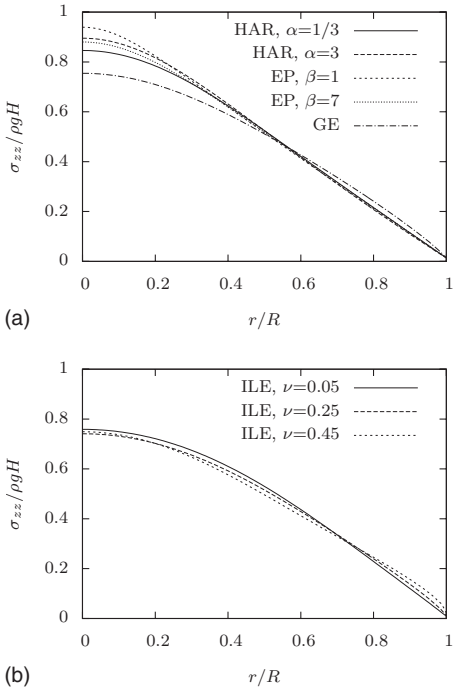

FIG. 11. Abaqus results for the stress at the bottom of a conical sand pile: hyperelastic models (top) and isotropic linear elasticity (bottom).

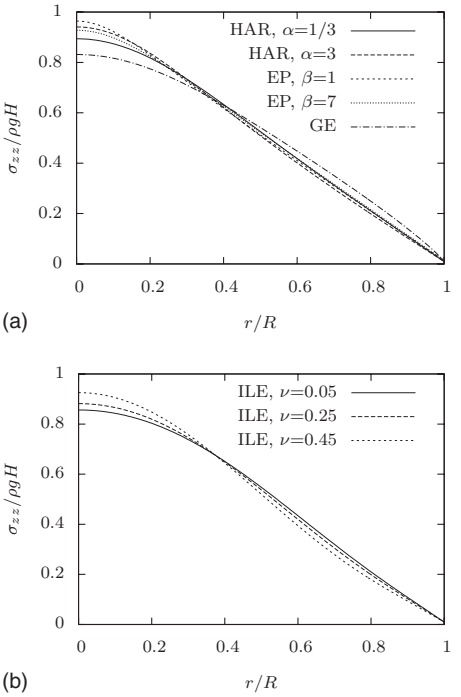

FIG. 12. Abaqus plane strain results for the stress at the bottom of a sand wedge: hyperelastic models (top) and isotropic linear elasticity (bottom).

free surface at the top of the pile where $P=0$; this is necessary to prevent divergence of $1/P$ and $1/\Delta$ terms in the stiffness matrix. The pressure applied at the surface ensures numerical stability, but does not impact the stress distributions away from the surface in any meaningful way, provided it is sufficiently small (10–20 Pa is used here). This is the same method employed in calculating stress distributions with GE [14,15]. Note, however, that this creates a problem if the objective is to predict yielding in the pile. Say, for example, that a pile is sufficiently steep that shear stresses exceed a critical fraction of the normal stresses, and we expect yielding to occur at the surface. Application of an additional normal stress at the surface will lower the stress ratio and provide stability in this case as well. It is worth noting that while the GE yield angle can be at most 26.5°, the model is applied to 33° sand piles without difficulty, presumably due to this additional normal force.

Unlike GE, in which ξ is fixed by the maximum yield angle, we are free to pick the values of the material constants α and β in the HAR and EP models. The same applies to A and B, though their values are not relevant for the current comparison; they scale the strains but do not change the stresses. Lacking any strain measurements from the current experiments, their value cannot be determined. The stress distributions for conical piles are shown in Fig. 11, and the plane strain results for wedge-shaped piles in Fig. 12. Since we are free to choose α and β in the HAR and EP models, several different values are tried for both conical and wedge-shaped piles. Their values do not strongly influence the stress distribution at the bottom of the pile in either case. The increase in stress from the edge of the pile toward the center is quite linear, as opposed to the experiments in which there is a significant leveling off [40]. Interestingly, none of the nonlinear models is appreciably different from isotropic linear elasticity (ILE) in this case; ILE is similarly independent of Young's modulus E, and only weakly dependent on Poisson's ratio ν. It gives a better match to experiment data than the EP and HAR models, particularly for the conical pile, though it still overestimates the peak height ($\sim$0.6 for conical and $\sim$0.8 for wedge-shaped piles [40]). None of the models produces a stress dip, though GE has reproduced one when a varying density was imposed [14].

C. Janssen Silo problem

Bräuer *et al.* [15] have calculated stress distributions in silos for comparison with the well known Janssen model [41]. The essential features of the Janssen model are saturating vertical stress with depth, the weight being supported by wall friction, and a constant ratio of vertical to horizontal stresses defined by the Janssen constant k_J,

$$\sigma_{rr} = k_J \sigma_{zz}. \tag{56}$$

For a silo of radius R and wall friction coefficient μ_f, the vertical stress is given by

$$\sigma_{zz} = \frac{\rho g R}{2 k_J \mu_f} + \left(\sigma_0 - \frac{\rho g R}{2 k_J \mu_f} \right) \exp\left(\frac{-2 k_J \mu_f}{R} z \right). \tag{57}$$

They find these assumptions well satisfied by GE, with σ_{zz} saturating for large depths z, and the ratio σ_{rr}/σ_{zz} becoming approximately constant; they find $k_J \sim 0.4$. With $\xi = 5/3$ fixed by the yield angle, the Janssen constant is fixed as well, though it is in practice found to vary by material [42]. The

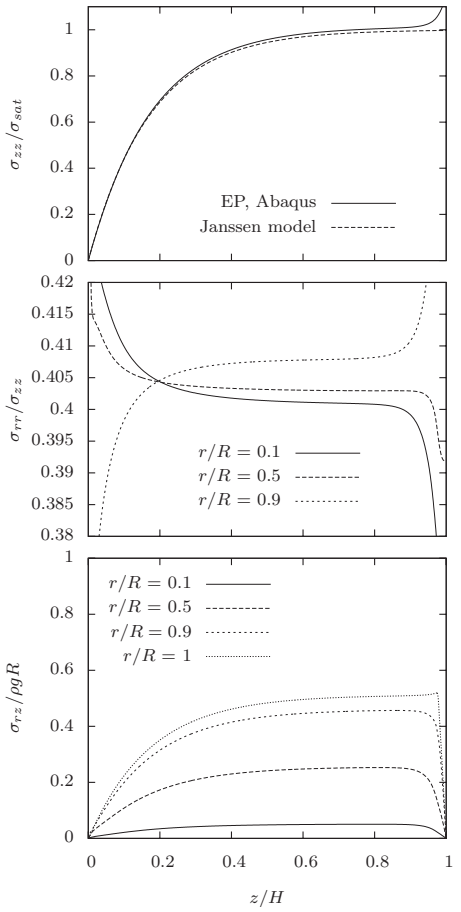

FIG. 13. Abaqus results for silo stresses using the EP model, with $\beta=3/2$.

Abaqus implementation of GE produces results consistent with those published [19].

Abaqus calculations using the EP and HAR models essentially produce the same behavior; the plots for the EP model are shown in Fig. 13, are similar to those reported for GE [15] and HAR [19], and compare well with the Janssen model until effects of the finite boundary dominate near $z=H$. Here the silo dimensions are $H=36$ m and $R=1$ m, and $\mu_f=0.2$. This is a very tall, narrow "silo," but such dimensions are necessary to observe the "saturating" behavior. The value of k_J used in plotting the Janssen equation is taken from the numerical results at the point $r/R=0.5$ and $z/H=0.5$. As reported for GE [15], the friction coefficient does not strongly influence the value of k_J.

While $\xi=5/3$ fixes k_J at ~ 0.4 for GE, in the EP and HAR models, we are free to choose β and α. The results are qualitatively similar to those in Fig. 13, but with k_J dependent on β or α. The relationships (shown in Fig. 14) are similar to the variation of the isotropic Poisson's ratio, ν_{iso}, obtained analytically [Eqs. (42) and (43)] and plotted in Figs. 3 and 4. That the Janssen concept of "vertical force redirection" is related to Poisson's ratio is perhaps not surprising; indeed, for isotropic linear elasticity at large z [43,44],

$$k_J = \frac{\nu}{1-\nu}. \tag{58}$$

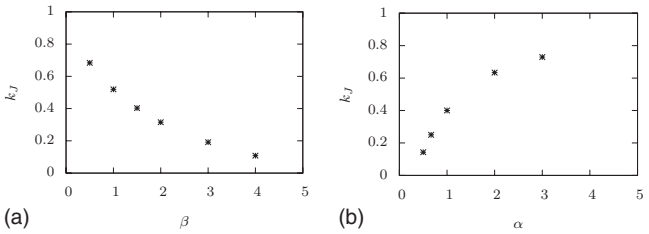

FIG. 14. Janssen's constant as a function of the material constant β for the EP model (left) and α for the HAR model (right). Values are taken at $r/R=0.5$ and $z/H=0.5$.

So, while the hyperelastic models reproduce the Janssen model, linear elasticity does as well. As a further point of comparison, consider a variation on this problem, in which a pressure equal to the saturation stress is applied at the surface of the silo (σ_0). In the Janssen equation (57), this gives $\sigma_{zz}/\sigma_{sat}=1$, independent of z. Experiments, on the other hand, find there is a significant "overshoot" of the saturated value, up to 20% [44,45]. While ILE was also found to produce an overshoot, it was 30–40 times smaller than the one observed experimentally, what Ovarlez *et al.* refer to as a "giant overshoot effect" [44]. They go on to speculate that stress-induced anisotropy may play a role in the overshoot, with a greater stiffness in the vertical direction due to the applied load. As the hyperelastic models possess stress-induced anisotropy, we might expect them to reproduce the effect. But the Abaqus results reveal that the overshoot in all three hyperelastic models is closer to that predicted by linear elasticity than observed in experiments. The GE and HAR models produce similar results, while in the EP model the decrease to the saturated value is much more gradual than for any of the other elastic models (Fig. 15).

D. Layer under a point load

The response function or Green's function of a granular material subject to a localized force perturbation was proposed as a fundamental test of granular mechanics [1]. Here there was an interest in resolving whether or not such systems were governed by elliptic or hyperbolic equations. While hyperbolic equations predict a double peaked response

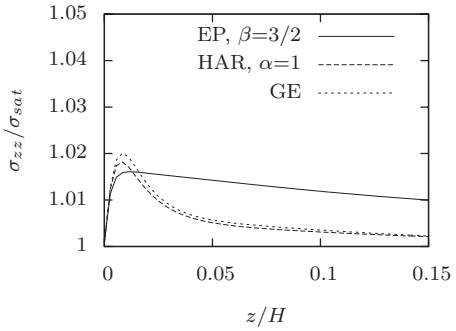

FIG. 15. Hyperelastic models for the "overshoot" in stress when a load equal to σ_{sat} is applied to the surface of the silo. Magnitudes of the overshoot are similar to those predicted by ILE, and smaller than observed in experiments [45].

function in two dimensions and a "ring" peak in three dimensions (as the forces propagate along characteristics), elliptic equations predict a single peak, with the half width increasing linearly with depth. Experiments [46–49] and simulations [50–52] seem to support the elliptic picture, at least for large, frictional, disordered systems under relatively light loads.

A first point of comparison here is the analytical solution for an infinite elastic half space [53], due to Boussinesq [54] and Cerutti [55]. With a force F applied to a point on its surface, the vertical stress at depth h and lateral distance r is given by

$$\sigma_{zz} = \frac{3F}{2\pi}\frac{h^3}{(r^2+h^2)^{5/2}}. \tag{59}$$

Here and throughout, we report instead the renormalized value

$$C \equiv \frac{h^2\sigma_{zz}}{F} = \frac{1}{\left(\frac{r^2}{h^2}+1\right)^{5/2}} \tag{60}$$

such that

$$\int_0^\infty 2\pi C(r')r'dr' = 1. \tag{61}$$

The Boussinesq-Cerutti solution depends only on the perturbing force and position; it has no dependence on the elastic constants. A finite system should be qualitatively similar, but will have some dependence on the elastic constants (i.e., Poisson's ratio) and the applied boundary conditions. As the shape of the profile found in experiments indicates elliptic governing equations, there have been attempts to model the problem using linear elasticity (both isotropic [47,49] and anisotropic [48]) and GE [15]. Serero *et al.* [47] find that the effect of a finite system size is primarily that it narrows the stress response function. The bottom boundary condition has a significant effect on the peak; in both cases, the z displacement, U_z, is zero, but a "smooth" bottom ($\sigma_{rz}=0$) produces a sharper peak than a "rough" bottom ($U_r=0$). Bräuer *et al.* claim that this boundary condition has little effect [15]; their curve for linear elasticity is also noticeably lower than both cases given by Serero *et al.* [47]. They find a response function for GE that is qualitatively similar, and narrower than the ILE and Boussinesq-Cerutti solutions. With ξ fixed at the maximum yield angle in GE, there are no parameters to adjust that would affect the shape or height of the peak. It is not clear then how GE might account for variations in the peak height observed experimentally [47,49]. Then again, Serero *et al.* find that the response function is not strongly influenced by the value of Poisson's ratio, except for inadmissible values greater than 1/2. Thus, isotropic linear elasticity was considered ill-suited to describe granular media, though qualitatively the behavior is indeed elliptic.

Following the problem description given by Bräuer *et al.*, Abaqus results have been obtained for the response function of the ILE, GE, EP, and HAR models. A small piston of diameter $D=1.456$ cm applies a pressure $P_1=500$ Pa at the surface of a granular disk of height $h=8$ cm. The radius of the disk R need only be large enough that the presence of the side walls does not significantly influence the response function at $h=8$ cm; $R=16$ cm is found to be sufficient, and the walls are considered rigid and smooth. In reality, the surface of the layer outside the piston is a free surface; but as before, this is problematic in the hyperelastic models, where zero pressure boundaries cannot be handled numerically. A surface force $P_0=150$ Pa is applied to avoid these issues, and the stress normalized accordingly:

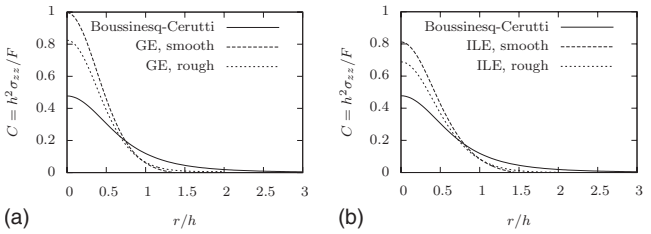

FIG. 16. Abaqus calculations of the response function for GE (top) and ILE (bottom). The presence of boundaries increases the peak height, and a frictionless bottom surface results in a higher peak than a rough surface (glued grains).

$$C \equiv \frac{4h^2}{P_1\pi D^2}(\sigma_{zz} - P_0 - \rho g h). \tag{62}$$

Results for GE and ILE are shown in Fig. 16. The ILE results are in quantitative agreement with those of Serero *et al.* [47], the curve narrowing due to finite system size and significantly more so for the smooth boundary condition. The same effects are evident in the GE calculation, in contrast with those reported by Bräuer *et al.* [15]; both the GE and ILE peaks are higher than the values presented there.

As the rough bottom boundary more accurately reflects the experiment conditions, this condition is employed in the EP and HAR calculations. Even so, both the EP and HAR models give peak heights significantly higher than predicted by GE and ILE, and observed in experiments (Fig. 17). The HAR model gives more reasonable results for increasing values of α, though recall it was *smaller* values of α that gave better results for the stress dependent elastic moduli. The EP model dramatically overestimates the peak height, by about an order of magnitude compared with some experiments, where the peak height ranged from ~0.3–0.8 [47]. Just as the ILE response proved insensitive to the value of ν, the EP

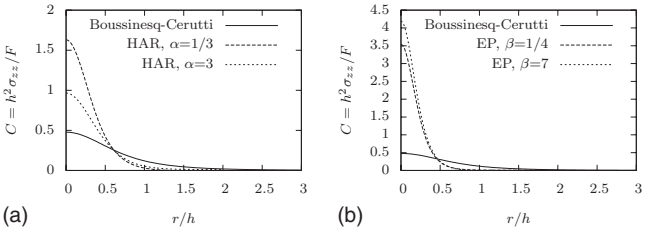

FIG. 17. Abaqus calculations of the response function for the HAR (top) and EP (bottom) models. The EP model predicts a much narrower response function than is observed, and is not particularly sensitive to the value of β.

response function varies little over the entire range of allowable values for β. Recall that $\beta=0$ is a mechanical stability limit for the EP model and corresponds to $\nu_{iso}=1/2$, while $\beta>8$ implies $\nu_{iso}<0$, which while theoretically admissible is not expected here.

So, of the hyperelastic models considered here, the EP model, which seemed to best capture the type of stress-induced anisotropy observed for Young's modulus, gives the least accurate response function by a wide margin. As the shape is relatively insensitive to the only adjustable constant β, there is no obvious way to resolve the discrepancy. The similar inability of isotropic linear elasticity to account for the range of observed data has prompted suggestions that fabric anisotropy be included in an anisotropic, linear elastic (ALE) model [46–48]. The simplest case would be a material possessing two Young's moduli, two Poisson's ratios, and a shear modulus. A similar "fabric" anisotropy could be incorporated into any of the hyperelastic models. But the caution of Serero *et al.* applies equally well here: taking five constants as fit parameters will almost certainly produce a good match to the experiment data. Without good reason to prescribe this sort of inherent anisotropy, there is probably little insight to be gained with such a model.

V. CONCLUSIONS

Three recently proposed hyperelastic models for granular materials have been investigated and compared with experiment data. The three different forms are all formulated to give elastic moduli that are power law functions of pressure, in accordance with a multitude of experiments. Aside from conserving energy and ensuring path independence, beginning with a scalar free energy, rather than simply a nonlinear stress-strain (or incremental stress-strain) relation, has a number of useful consequences for granular materials. Among these are stress-induced anisotropy, coupling between shear and normal stresses that gives rise to shear dilatancy, and (in two of the three models) a prohibition of tensile states and a limit on the ratio of stress invariants.

In the case of granular elasticity (GE), the limiting stress ratio is the result of mechanical instability. While this gives appropriate limits on the stress ratio for a triaxial test, the yield angle of a plane has an unexpected maximum of $\phi \approx 26.5°$ for Hertz contacts, lower still for higher power laws (e.g., $a=1$).

Models proposed by Einav and Puzrin (EP) and Houlsby, Amorosi, and Rojas (HAR) employed similar ideas based on the Gibbs (rather than Helmholtz) free energy. While elastic moduli obtained from each model are power laws when plotted against the mean stress, they have rather different dependence on the individual stress components, and generally do not agree with forms well established by experiments. An exception is Young's modulus in the EP model, which varies only weakly with the out of plane normal stresses.

All three hyperelastic models were implemented in the finite element code Abaqus for comparison with each other and a series of experiments originally considered by Jiang and Liu: stress distributions under sand piles and silos, and the granular response function. Results were qualitatively similar for all models. For both sand piles and the response function, peak stresses were very insensitive to the elastic constants, and were not able to account for the variability of peak heights observed in experiments. These may be largely due to preparation dependence of the piles and layers, and some mechanism to account for this should be added to models of this type. Allowing for varying density is one possibility, and it was shown previously that this could account for the sand pile stress dip that is sometimes observed.

The hyperelastic models match the Janssen model for silos, with the vertical stress saturating with depth due to wall friction, but this behavior is equally well captured by isotropic linear elasticity. If a pressure equal to the saturated value is added to the surface of the silo, the Janssen model gives $\sigma_{zz}/\sigma_{sat}=1$ everywhere, while a substantial "overshoot" (up to 20%) of the saturated stress is observed in experiments. Linear elasticity predicts a very small overshoot, less than 1%. All three hyperelastic models give an overshoot of around 2%, closer to the linear elastic case than reality. This may indicate that the large overshoot is not due to stress-induced anisotropy, or at least that the present models do not predict this anisotropy correctly.

Finally, it should be noted that many yield surfaces depend on the third stress invariant, while the Drucker-Prager surface predicted by GE does not. As the observed stress-induced anisotropy in the shear moduli can also only result from a three-invariant model, this may be a point for further investigation.

ACKNOWLEDGMENTS

This paper has been authored under Battelle Energy Alliance, LLC under Contract No. DE-AC07-05ID14517 with the U.S. Department of Energy.

[1] P.-G. de Gennes, Rev. Mod. Phys. **71**, S374 (1999).
[2] M. Zytynski, M. F. Randolph, R. Nova, and C. P. Wroth, Int. J. Numer. Analyt. Meth. Geomech. **2**, 87 (1978).
[3] G. T. Houlsby, Comput. Geotech. **1**, 3 (1985).
[4] I. F. Collins and G. T. Houlsby, Proc. R. Soc. London, Ser. A **453**, 1975 (1997).
[5] G. T. Houlsby and A. M. Puzrin, Int. J. Plast. **16**, 1017 (2000).
[6] G. T. Houlsby and A. M. Puzrin, *Principles of Hyperplasticity: An Approach to Plasticity Theory Based on Thermodynamic Principles* (Springer, London, 2006).
[7] J. Duffy and R. D. Mindlin, ASME J. Appl. Mech. **24**, 585 (1957).
[8] H. B. Callen, *Thermodynamics and an Introduction to Thermostatistics*, 2nd ed. (Wiley, New York, 1985).
[9] Y. Jiang and M. Liu, Phys. Rev. Lett. **91**, 144301 (2003).
[10] J. D. Goddard, Proc. R. Soc. London, Ser. A **430**, 105 (1990).

[11] P.-G. de Gennes, Europhys. Lett. **35**, 145 (1996).
[12] Y. Jiang and M. Liu, Phys. Rev. Lett. **93**, 148001 (2004).
[13] Y. M. Jiang and M. Liu, in *Powders and Grains 2005*, edited by R. García-Rojo, H. J. Herrmann, and S. McNamara (A. A. Balkema, Leiden, The Netherlands, 2005), pp. 433–436.
[14] D. O. Krimer, M. Pfitzner, K. Bräuer, Y. Jiang, and M. Liu, Phys. Rev. E **74**, 061310 (2006).
[15] K. Bräuer, M. Pfitzner, D. O. Krimer, M. Mayer, Y. Jiang, and M. Liu, Phys. Rev. E **74**, 061311 (2006).
[16] Y. Jiang and M. Liu, Eur. Phys. J. E **22**, 255 (2007).
[17] Y. Jiang and M. Liu, Phys. Rev. E **77**, 021306 (2008).
[18] D. C. Drucker and W. Prager, Q. Appl. Math. **10**, 157 (1952).
[19] P. W. Humrickhouse, Ph.D. thesis, University of Wisconsin-Madison, 2009.
[20] P. W. Humrickhouse, in *Powders and Grains 2009*, edited by M. Nakagawa and S. Luding (American Institute of Physics, Melville, New York, 2009), pp. 1104–1107.
[21] Y. Grasselli and H. J. Herrmann, Physica A **246**, 301 (1997).
[22] P. Boltenhagen, Eur. Phys. J. B **12**, 75 (1999).
[23] I. Einav and A. M. Puzrin, J. Geotech. Geoenviron. Eng. **130**, 81 (2004).
[24] G. T. Houlsby, A. Amorosi, and E. Rojas, Geotechnique **55**, 383 (2005).
[25] E. Hoque, F. Tatsuoka, and T. Sato, Geotech. Test. J. **19**, 411 (1996).
[26] L. AnhDan, J. Koseki, and T. Sato, Geotech. Test. J. **29**, GTJ100221 (2006).
[27] L. AnhDan and J. Koseki, Soils Found. **45**, 21 (2005).
[28] R. Bellotti, M. Jamiolkowski, D. C. F. Lo Presti, and D. A. O'Neill, Geotechnique **46**, 115 (1996).
[29] V. Fiorvante, Soils Found. **40**, 129 (2000).
[30] B. O. Hardin and G. E. Blandford, J. Geotech. Eng. **115**, 788 (1989).
[31] N. HongNam, J. Koseki, and T. Sato, Geotech. Test. J. **31**, 1 (2007).
[32] E. Hoque and F. Tatsuoka, Soils Found. **38**, 163 (1998).
[33] E. Hoque and F. Tatsuoka, Geotechnique **54**, 429 (2004).
[34] G.-L. Jiang, F. Tatsuoka, A. Flora, and J. Koseki, Geotechnique **47**, 509 (1997).
[35] Y. Kohata, F. Tatsuoka, L. Wang, G.-L. Jiang, E. Hoque, and T. Kodaka, Geotechnique **47**, 563 (1997).
[36] R. Kuwano and R. J. Jardine, Geotechnique **52**, 727 (2002).
[37] S. K. Roesler, Proc. Am. Soc. Civ. Eng. **105**, 871 (1979).
[38] T. G. Thomann and R. D. Hryciw, Geotech. Test. J. **13**, 97 (1990).
[39] *Abaqus Version 6.8 Documentation Collection*, Dassault Systèmes (2008), http://simulia.com.
[40] L. Vanel, D. Howell, D. Clark, R. P. Behringer, and E. Clément, Phys. Rev. E **60**, R5040 (1999).
[41] H. A. Janssen, Z. Ver. Dtsch. Ing. **39**, 1045 (1895).
[42] V. Sundaram and S. C. Cowin, Powder Technol. **22**, 23 (1979).
[43] P. Evesque and P.-G. de Gennes, C. R. Acad. Sci., Ser. IIb: Mec., Phys., Chim., Astron. **326**, 761 (1998).
[44] G. Ovarlez, C. Fond, and E. Clément, Phys. Rev. E **67**, 060302(R) (2003).
[45] G. Ovarlez and E. Clément, Eur. Phys. J. E **16**, 421 (2005).
[46] G. Reydellet and E. Clément, Phys. Rev. Lett. **86**, 3308 (2001).
[47] D. Serero, G. Reydellet, P. Claudin, É. Clément, and D. Levine, Eur. Phys. J. E **6**, 169 (2001).
[48] A. P. F. Atman, P. Brunet, J. Geng, G. Reydellet, P. Claudin, R. P. Behringer, and E. Clément, Eur. Phys. J. E **17**, 93 (2005).
[49] A. P. F. Atman, P. Brunet, J. Geng, G. Reydellet, G. Combe, P. Claudin, R. P. Behringer, and E. Clément, J. Phys.: Condens. Matter **17**, S2391 (2005).
[50] C. Goldenberg and I. Goldhirsch, Phys. Rev. Lett. **89**, 084302 (2002).
[51] C. Goldenberg and I. Goldhirsch, Nature (London) **435**, 188 (2005).
[52] C. Goldenberg and I. Goldhirsch, Phys. Rev. E **77**, 041303 (2008).
[53] K. L. Johnson, *Contact Mechanics* (Cambridge University Press, Cambridge, England, 1985).
[54] J. Boussinesq, *Application des Potentials à l'etude de l'équilibre et du Mouvement des Solides Élastiques* (Gauthier-Villars, Paris, 1885).
[55] V. Cerruti, Atti R. Accad. Naz. Lincei, Mem. Cl. Sci. Fis., Mat. Nat. **13**, 81 (1882).